Octupole deformation in neutron-rich actinides and superheavy nuclei and the role of nodal structure of single-particle wavefunctions in extremely deformed structures of light nuclei.

A. V. Afanasjev[1,3]**, H. Abusara**[2]**, S. E. Agbemava**[1]

[1]Department of Physics and Astronomy, Mississippi State University, MS 39762, USA
[2]Physics Department, Birzeit University, Birzeit, Palestine

E-mail: [3]`Anatoli.Afanasjev@gmail.com`

Abstract. Octupole deformed shapes in neutron-rich actinides and superheavy nuclei as well as extremely deformed shapes of the $N \sim Z$ light nuclei have been investigated within the framework of covariant density functional theory. We confirmed the presence of new region of octupole deformation in neutron-rich actinides with the center around $Z \sim 96, N \sim 196$ but our calculations do not predict octupole deformation in the ground states of superheavy $Z \geq 108$ nuclei. As exemplified by the study of ^{36}Ar, the nodal structure of the wavefunction of occupied single-particle orbitals in extremely deformed structures allows to understand the formation of the α-clusters in very light nuclei, the suppression of the α-clusterization with the increase of mass number, the formation of ellipsoidal mean-field type structures and nuclear molecules.

1. Introduction

The concepts of nuclear shape and shape coexistence are the centerpieces of low energy nuclear physics [1]. These shapes are connected with the symmetry breaking of the nuclear mean field and manifest themselves in different forms. Breaking of spherical symmetry leads to deformed shapes, the simplest ones are axial quadrupole deformed shapes. However, the change of their elongation leads to different classes of nuclear shapes such as normal-, super-, hyper- and megadeformed ones. Next step is breaking of the symmetry of the mean field in the plane perpendicular to the axis of symmetry. This leads to reflection asymmetric (octupole deformed) shapes. The density functional theory [2, 3] provides a natural framework for the description of different classes of nuclear shapes across whole nuclear chart. This manuscript presents recent results obtained in the studies of nuclear shapes within the framework of covariant density functional theory (CDFT) [3]. It is focused on two issues discussed below and covers two extreme ends of the nuclear chart.

First issue is the role of octupole deformation in the ground states of neutron-rich actinides and superheavy nuclei. The global investigation of Ref. [4] performed with the DD-PC1 [5] and NL3* [6] covariant energy density functionals (CEDFs) found the presence of the island of octupole deformation in the region with center around $Z \sim 96, N \sim 196$. In order to estimate theoretical uncertainties in model predictions, we performed additional studies with the DD-ME2 [7] and PC-PK1 [8] CEDFs. This study covers not only the above mentioned region but also extends to superheavy nuclei for which the calculations have been performed with all four functionals. Note that the octupole deformation in the ground states of superheavy nuclei has not been studied in the CDFT framework before our investigation.

The second issue is the role of the single-particle degrees of freedom in the formation of extremely deformed shapes of rotating nuclei and in the transition from ellipsoidal mean field type configurations towards nuclear molecules. A systematic investigation of extremely deformed structures at high spin has been performed in Refs. [9, 10] for the $N \approx Z$ nuclei with $Z = 14 - 24$. These studies show that particle-hole excitations within the same nucleus lead to the formation of different nuclear shapes starting from spherical ones via normal-deformed to super-, hyper- and megadeformed ones. Among these extremely deformed shapes there are the examples of ellipsoidal mean-field type structures, nuclear molecules and clustered configurations. Thus, it is important to understand what role single-particle states (and, in particular, the nodal structure of their wavefunctions)

are playing in the formation of such structures. To our knowledge, this aspect of the nuclear many-body problem has not been studied so far.

The paper is organized as follows. Section 2 describes the main results obtained in the study of octupole deformation in the ground states of neutron-rich actinides and superheavy nuclei. Sec. 3 is devoted to the discussion of the role of the single-particle degrees of freedom in clusterization and in the formation of extremely deformed structures and nuclear molecules; this is done on the example of ^{36}Ar. Finally, Sec. 4 summarizes the results of our work.

2. Octupole deformation in neutron-rich actinides and superheavy nuclei

The calculations have been performed in the Relativistic-Hartree-Bogoliubov (RHB) approach using parallel computer code RHB-OCT developed in Ref. [4]. In the calculations, the constraints on quadrupole and octupole moments are employed. In order to avoid the uncertainties connected with the definition of the size of the pairing window [11], the separable form of the finite range Gogny pairing interaction introduced by Tian et al [12] is used in the calculations.

The effect of octupole deformation is characterized by the quantity ΔE_{oct} defined as

$$\Delta E_{oct} = E^{oct}(\beta_2, \beta_3) - E^{quad}(\beta'_2, \beta'_3 = 0) \qquad (1)$$

where $E^{oct}(\beta_2, \beta_3)$ and $E^{quad}(\beta'_2, \beta'_3 = 0)$ are the binding energies of the nucleus in two local minima of potential energy surface (PES); the first minimum corresponds to octupole deformed shapes and second one to the shapes with no octupole deformation. The quantity $|\Delta E_{oct}|$ represents the gain of binding due to octupole deformation. It is also an indicator of the stability of the octupole deformed shapes. Large $|\Delta E_{oct}|$ values are typical for well pronounced octupole minima in the PES; for such systems the stabilization of static octupole deformation is likely. On the contrary, small $|\Delta E_{oct}|$ values are characteristic for soft (in octupole direction) PES typical for octupole vibrations.

The RHB results for octupole deformed nuclei are summarized in Fig. 1. The present investigation confirms the predictions of Ref. [4] about the existence of the region of octupole deformation centered around $Z \sim 96, N \sim 196$ obtained with the DD-PC1 and NL3* functionals. Most of the CEDFs predict the size of this region in the (Z, N) plane larger than the one of the experimentally known region at $Z \sim 92, N \sim 136$. On the other hand, the impact of octupole deformation on the binding energies of the nuclei in these two regions are comparable. The search for octupole deformation in the ground states of even-even superheavy $Z =$
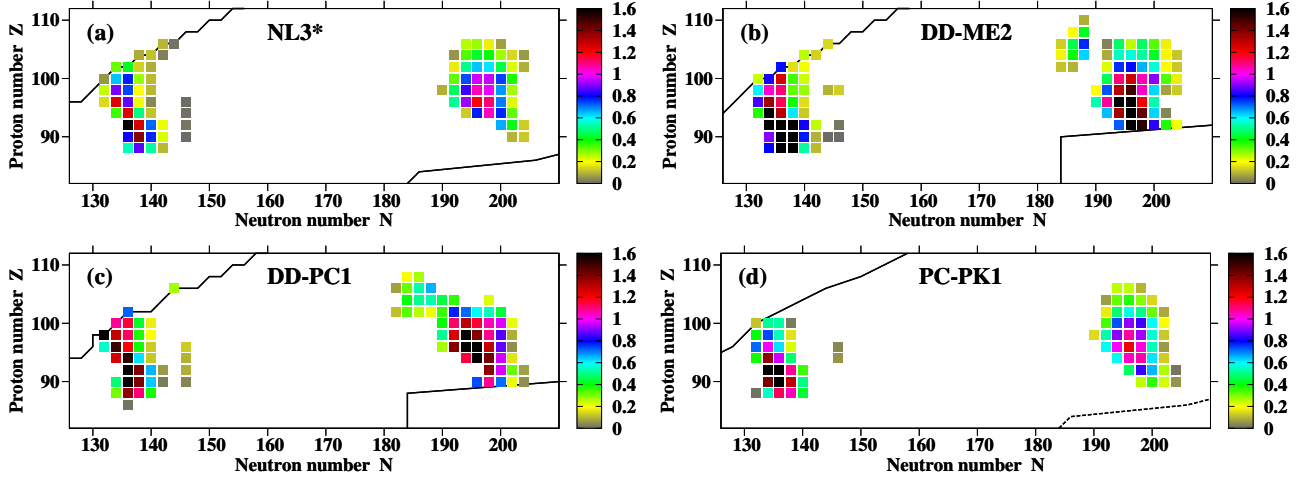
Figure 1. Octupole deformed nuclei in the part of nuclear chart under study for indicated covariant energy density functionals. Only nuclei with non-vanishing ΔE^{oct} are shown by squares; the colors of the squares represent the values of $|\Delta E^{oct}|$ (in MeV) (see colormap). The two-proton and two-neutron drip lines are displayed by solid black lines. From Ref. [13].
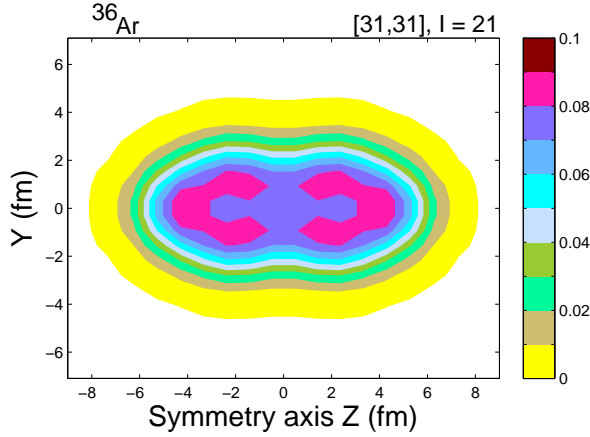

Figure 2. Total neutron density [in fm^{-3}] of the megadeformed [31,31] configuration in ^{36}Ar obtained in the CRMF calculations with the NL3* functional.

$108 - 126$ nuclei with neutron numbers from the two-proton drip line up to neutron number $N = 210$ has been performed in the CDFT framework for the first time. With the exception of two $Z = 108$ (two $Z = 108$ and one $Z = 110$) octupole deformed nuclei in the calculations with CEDF DD-PC1 (DD-ME2), no octupole deformed shapes in the ground states of these nuclei have been found.

It is important to compare the CDFT predictions with the ones obtained in non-relativistic theories. Similar region of octupole deformation is predicted also in Skyrme DFT [14] and microscopic+macrosscopic (mic+mac) [15] calculations. However, it is centered at $Z \sim 100, N \sim 190$ in the Skyrme DFT calculations and at $Z \sim 100, N \sim 184$ in mic+mac calculations. The

existing Gogny DFT calculations [16] do not extend below $Z = 98$ and beyond $N = 190$; however, the trends seen in these calculations do not suggest the existence of the region of octupole deformation in very neutron rich actinides. The predictions for octupole deformation in the ground states of superheavy $Z \geq 108$ nuclei differ drastically. Both CDFT and Skyrme DFT do not predict octupole deformation in these nuclei. On the contrary, large region of octupole deformation is predicted in superheavy nuclei in the mic+mac and Gogny DFT calculations. These differences in the location of the islands of octupole deformed nuclei are due to the differences in the underlying single-particle structure which exist among the models in actinides and superheavy nuclei [17, 18, 19].

Note that the accounting of octupole deformation in the ground states of the $Z \sim 98, N \sim 196$ nuclei is essential for the modeling of fission recycling in neutron star mergers [20, 21] since the gain in binding energy of the ground states due to octupole deformation will increase the fission barrier heights as compared with the case when octupole deformation is neglected. These changes in binding energy of the ground states and fission barriers affect the r-process [20, 21]. It is also necessary to recognize that the present results are restricted to the mean field level. The methods beyond mean field such as quadrupole-octupole collective Hamiltonian [23] or generator coordinate method including octupole deformation [22] have to be employed to define excitation spectra and transition rates of these nuclei.

3. The role of single-particle degrees of freedom in clusterization and nuclear molecules: an example of megadeformed [31,31] configuration in ^{36}Ar.

The calculations in the cranked relativistic mean field (CRMF) [9] and cranked Nilsson-Strutinsky (CNS) [24] frameworks clearly indicate ^{36}Ar as one of the best candidates for the observation of the hyper- (HD) and megadeformation (MD) at high spin. The observed superdeformed band terminates at spin $I = 16^+$ [25]. The population of the HD and MD states is very likely if it will be possible to bring higher (than $16\hbar$) angular momentum into the system [9]. For example, the MD [31,31] configuration is predicted to become yrast at spin $I \geq 21\hbar$ (see Fig. 21 in Ref. [9]). Here the calculated configurations are labeled by shorthand $[n_1 n_2, p_1 p_2]$ labels, where n_1 and n_2 (p_1 and p_2) are the number of neutrons (protons) in the $N = 3$ and 4 intruder/hyperintruder orbitals.

Fig. 2 shows the total neutron density distribution of this configuration at the spin at which this configuration becomes yrast. The proton density distribution is almost the same; thus it is not shown here. One can see clear fingerprints of the molecular structure in this density distribution; two clusters with high densities in their near-central region are separated by a well-established neck. It looks as a pair of two octupole (pear-shaped) deformed ^{18}F nuclei. This is one of the forms of the clusterization predicted in nuclei [26]. It is reasonable to expect that single-particle degrees of freedom play an important role in the formation of molecular structures. However, to our knowledge this question has never been studied in detail in nuclei with $A \geq 20$ and in rotating nuclei. This is contrary to the situation in very light nuclei in which the connection between α clusterization and underlying single-particle structure has been explored for non-rotating nuclei in detail in a number of publications (see, for example, Refs. [27, 28, 29, 30]). For example, the buildup of total nucleonic density of the α cluster structures in the Be and C isotopes by means of the single-particle contributions has been explored within the CDFT framework in Ref. [29].

To better understand the role of the single-particle states and their nodal structure in the buildup of total nucleonic density in molecular states we consider the density distributions of the neutron states with signature $r = -i$ occupied in the MD [31,31] configuration of ^{36}Ar. The calculations are performed in the CRMF framework [3] using the NL3* CEDF [6] and their results are shown in Figs. 3 and 4. The one-dimensional rotation in the CRMF framework is along the x-axis [3]. Note that the structure of the yrast and near-yrast states in ^{36}Ar has been studied in detail in Ref. [9]. In addition, the current distributions

$\mathbf{j}^n(\mathbf{r})$ produced by these states are shown by arrows in Figs. 3 and 4. As discussed in detail in Ref. [31]), these currents have a significant impact on rotational properties of the nuclei.

The single-particle orbitals are labeled by the asymptotic quantum numbers $[Nn_z\Lambda]\Omega$ (Nilsson quantum numbers) of the dominant component of the wave function. The shape of the [31,31] MD configuration is nearly axial with large quadrupole β_2 deformation (Fig. 23 in Ref. [9]). As a result, the weight of the dominant component exceed 75% of the total wavefunction for the majority of the states. The only exceptions are the [440]1/2, [330]1/2 and [321]3/2 states for which the weights of the dominant component are 55%, 62% and 54%, respectively.

The single-particle states can be separated into several groups according to general features of their density distribution. One of the groups is represented by the $[NN0]1/2$ states for which the maximum of the density distribution in the density clusters is located at the axis of symmetry. The density clusters are spheroidal or elipsoidal in shape and the wavefunction does not have nodes in the direction perpendicular to the symmetry axis. The number of the density clusters in these states is equal to $N + 1$ and the maximum density is always observed in the density clusters which are located in the polar region of the nucleus. Note that the maximum density in the clusters decreases with the increase of N. The wave function is well localized in such states with $N = 0, 1$ and 2 [Figs. (3)a-f]; among all considered single-particle states these are the ones with the highest densities in the center of the density clusters. This is a reason why they play an important role in the α-clusterization; they are responsible for the formation of two α-cluster state in ^{8}Be [26, 29] and linear chain of three α-particles in ^{12}C [27, 32].

The density distributions of other single-particle orbitals are characterized by different nodal structure. Their wavefunctions have a single node in the direction perpendicular to the axis of symmetry, which in ideal case of no state mixing would lead to zero density at the axis of symmetry. The [101]3/2 and [101]1/2 orbitals show very similar density distributions of doughnut type in which the maximum of density is located in the equatorial plane [Figs. (3)j-l and Figs. (4)a-c]. These two orbitals at spin zero differ only in the orientation of the single-particle spin along the symmetry axis which has only moderate impact on the density distribution. At no rotation, these doughnut density distributions are axially symmetric. However, the rotation leads to a different redistribution of the neutron matter for the $r = \pm i$ branches of the single-particle orbital resulting in an asymmetric doughnut density distributions in which the density depends on asimuthal angle. For example, the matter is moved
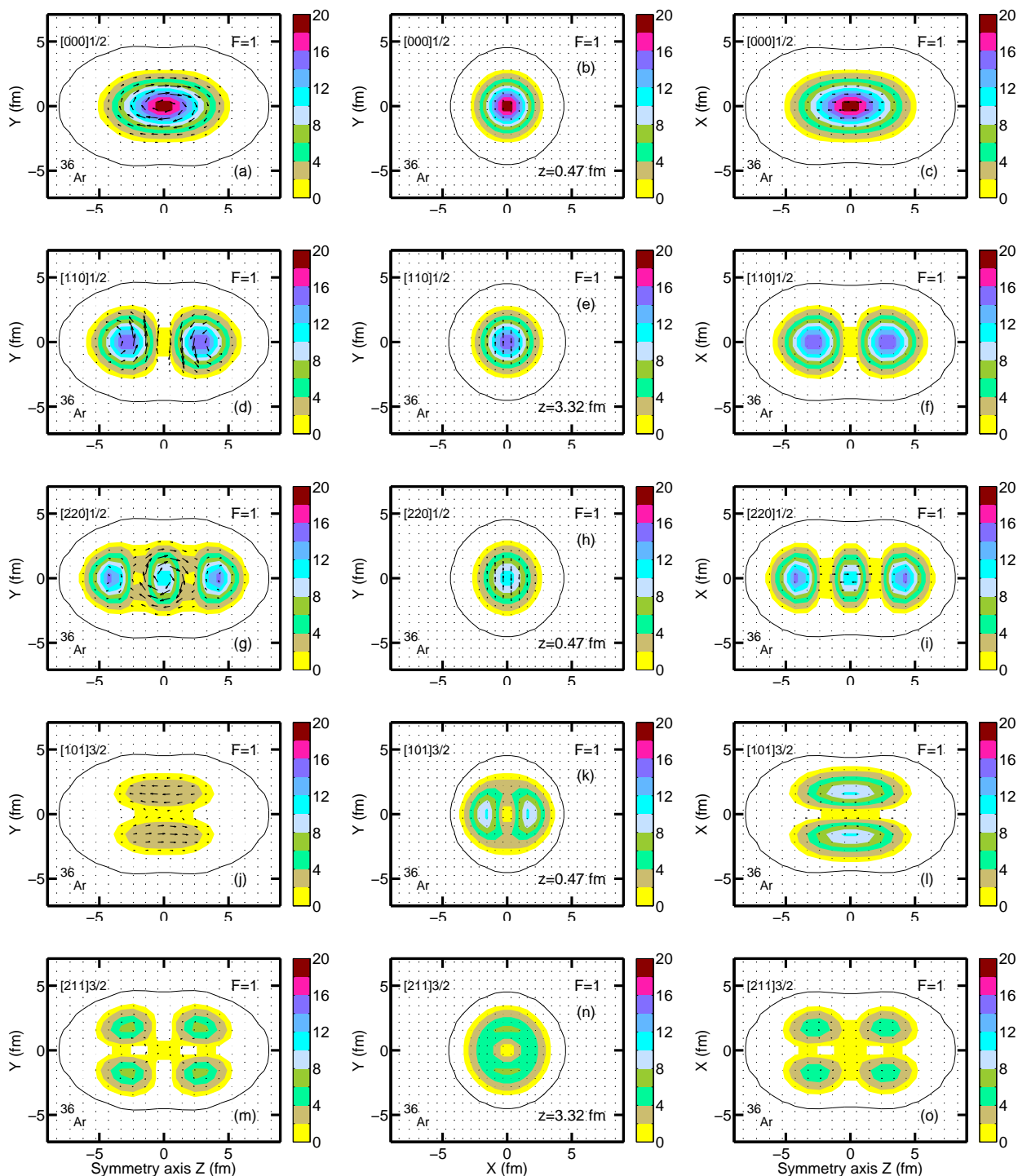
Figure 3. The single-neutron density distributions [in 0.001 fm^{-1}] due to the occupation of the indicated Nilsson states with signature $r = -i$ in the megadeformed [31,31] configuration of ^{36}Ar obtained in the calculations with the NL3* CEDF. To give a full 3-dimensional representation of the single-particle density distributions, they are plotted in the xz and yz planes at the positions of the Gauss-Hermite integration points in the y and x directions closest to zero, namely, at $x = y = 0.310$ fm, and in the xy plane at the Gauss-Hermite integration point in the z-coordinate (the value of this coordinate is shown in middle panels) which gives the largest density. The states are shown from the bottom of nucleonic potential in the same sequence as they appear in the routhian diagram of this configuration. The colormap shows the densities as multiplies of 0.001 fm^{-3}. The shape and size of the nucleus are indicated by black solid line which corresponds to total neutron density of $\rho = 0.001$ fm^{-3}. In addition, the current distributions $\mathbf{j}^n(\mathbf{r})$ produced by these states are shown by arrows. The currents in panel (a) are plotted at arbitrary units for better visualization. In other panels they are normalized to the currents in above mentioned panel by using factor F.
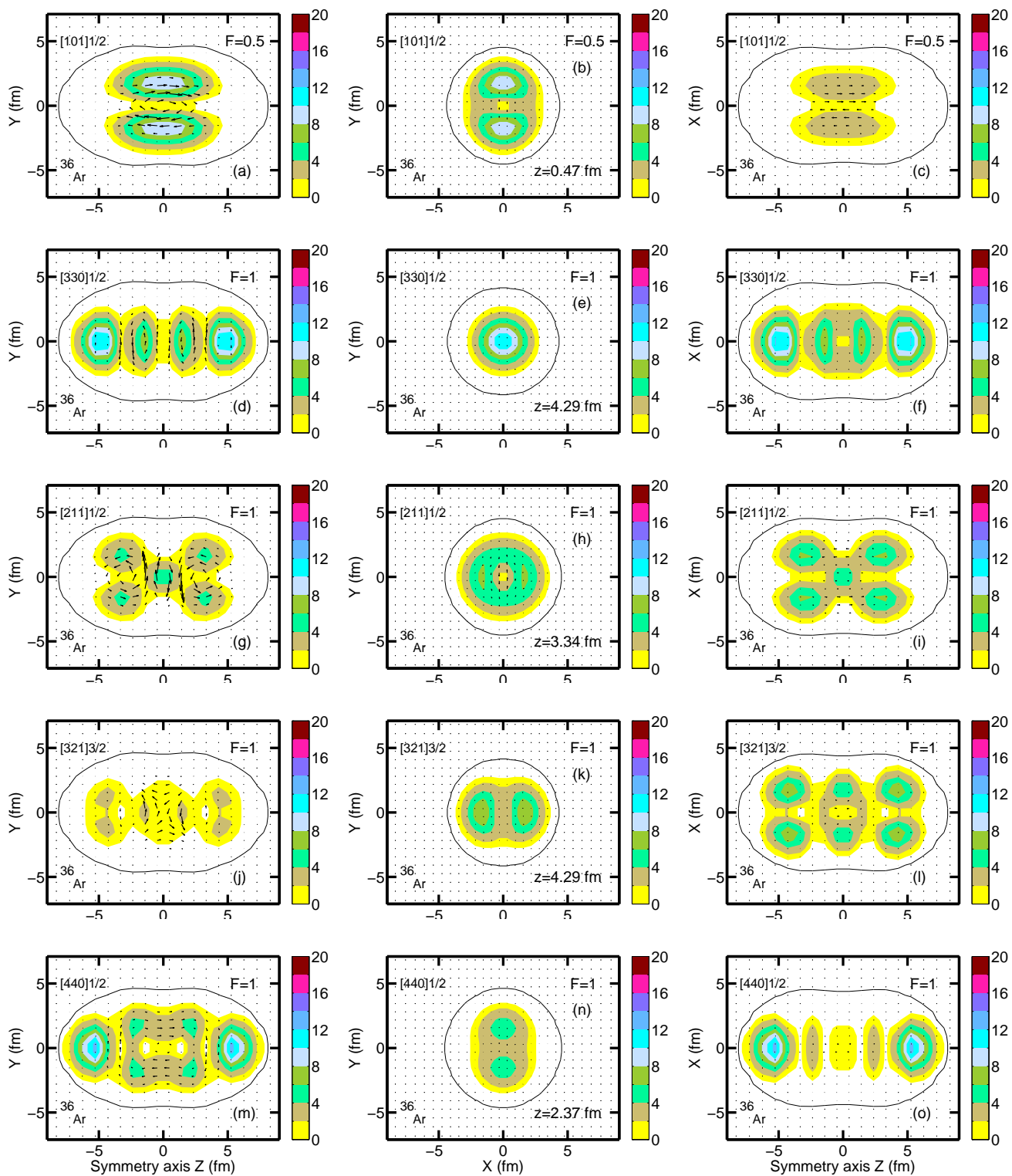
Figure 4. The same as Fig. 3 but for remaining occupied neutron orbitals with $r = -i$ in the megadeformed [31,31] configuration of ^{36}Ar.

away from the xz plane in the $\pm y$ directions for the [101]1/2($r = -i$) orbital [see Figs. (4)a-c]. For the [101]1/2($r = +i$), this transition proceeds from the yz

plane in the $\pm x$ direction (similar to what is seen for the [101]3/2($r = -i$) orbital in Fig. (3)j-l).

The wavefunction of the [211]3/2 orbital has one

radial node and one node in the z-direction. As a result, its density distribution is the combination of two asymmetric density rings located symmetrically with respect of equatorial plane [see Figs. (4)m-o]. The [211]1/2 orbital has similar structure with two density rings but in addition it has a spheroidal density cluster in the center of the nucleus (see Figs. 4m-o). Three asymmetric density rings are seen in the [321]3/2 orbital (see Figs. 4j-l). This asymmetry (dependence of the density on asimuthal angle) is due to rotation of the system; density rings in the [211]3/2, [211]1/2 and [321]3/2 orbitals are axially symmetric at no rotation.

The observed features of the single-particle density distributions coming from the nodal structure of the wavefunction allow to understand in a relatively simple way the necessary conditions for the α-clusterization and for the formation of nuclear molecules and ellipsoidal mean field type shapes. Two factors play an important role here: the degree of the localization of the wavefunction and the type of the density clusters formed by the single-particle orbital. It is clear that for the α-clusterization the single-particle density clusters should be compact (well localized), should have spheroidal density distribution and overlap in space. These conditions are satisfied only for the lowest states of the $[NN0]1/2$ type with $N = 0, 1$ and 2 which are active in the α-cluster structures of very light nuclei [26, 33, 32]. With increasing particle number the orbitals with doughnut and multiply ring type density distributions become occupied. These states are substantially less localized; the maximum of the density in such structures is typically much smaller than the maximum of the density in the lowest $[NN0]1/2$ orbitals. In addition, such density distributions (doughnuts and rings) are incompatible with α-clusters. Thus, dependent on the nucleonic configuration they contribute into the building of either mean field structures or nuclear molecules. To build the later structures one has to move the matter from the neck (equatorial) region into the polar regions of the nucleus. Specific particle-hole excitation removing particles from (preferentially) doughnut type orbitals or from the orbitals which have a density ring in an equatorial plane into the orbitals (preferentially of the $[NN0]1/2$ type) which build the density mostly in the polar regions will lead to more pronounced nuclear molecules. This is what exactly happens in ^{36}Ar on the transition from the hyperdeformed [4,4] configuration, which has ellipsoidal mean field like density distribution [see Fig. 24b in Ref. [9]]), to the MD [31,31] configuration which is an example of nuclear molecule [see Fig. 24c in Ref. [9] and Fig. 2 in the present paper]. This transition involves the proton and neutron particle-hole excitations from the 3/2[321] orbital into the [440]1/2 orbital.

4. Conclusions

Nuclear shapes of two kinds at the ground state and in rotating nuclei have been studied within the covariant density functional theory.

Octupole shapes at the ground state have been searched in actinides and superheavy nuclei. The presence of the new region of octupole deformation in neutron-rich actinides with the center around $Z \sim 96, N \sim 196$ suggested in Ref. [4] has been confirmed. However, our calculations do not predict octupole shapes in superheavy $Z \geq 108$ nuclei. The similarities and differences in the predictions of octupole deformation between non-relativistic and relativistic DFTs have been discussed.

The role of the nodal structure of the wavefunction of occupied single-particle orbitals in extremely deformed structures of the $N \sim Z$ nuclei has been investigated in detail on the example of megadeformed configuration in ^{36}Ar. It allows to understand the formation of the α-clusters in very light nuclei, the suppression of the α-clusterization with the increase of mass number, the formation of ellipsoidal mean-field type structures and nuclear molecules. The particle-hole excitations between different types of the single-particle orbitals explain the transition between the later two classes of nuclear shapes.

5. Acknowledgements

6. References

[1] S. G. Nilsson and I. Ragnarsson, Shapes and shells in nuclear structure, (Cambridge University Press, 1995).

[2] M. Bender, P.-H. Heenen and P.-G. Reinhard, Rev. Mod. Phys. 75, 121 (2003).

[3] D. Vretenar, A. V. Afanasjev, G. A. Lalazissis and P. Ring, Phys. Rep. 409, 101 (2005).

[4] S. E. Agbemava, A. V. Afanasjev and P. Ring, Phys. Rev. C 93, 044304 (2016).

[5] T. Nikšić, D. Vretenar and P. Ring, Phys. Rev. C 78, 034318 (2008).

[6] G. A. Lalazissis, S. Karatzikos, R. Fossion, D. Peña Arteaga, A. V. Afanasjev and P. Ring, Phys. Lett. B761, 36 (2009).

[7] G. A. Lalazissis, T. Nikšić, D. Vretenar and P. Ring, Phys. Rev. C 71, 024312 (2005).

[8] P. W. Zhao, Z. P. Li, J. M. Yao and J. Meng, Phys. Rev. C 82, 054319 (2010).

[9] D. Ray and A. V. Afanasjev, Phys. Rev. C 94, 014310 (2010).

[10] A. V. Afanasjev and D. Ray, J. Phys: Conf. Ser. 863, 012502 (2017).

[11] S. Karatzikos, A. V. Afanasjev, G. A. Lalazissis and P. Ring, Phys. Lett. B 689, 72 (2010).

[12] Y. Tian, Z. Y. Ma and P. Ring, Phys. Lett. B 676, 44 (2009).

[13] S. E. Agbemava and A. V. Afanasjev, submitted to Phys. Rev. C

[14] J. Erler, K. Langanke, H. P. Loens, G. Martinez-Pinedo and P.-G. Reinhard, Phys. Rev. C 85, 025802 (2012).

[15] P. Möller, J. R. Nix, W. D. Myers and W. J. Swiatecki, At. Data Nucl. Data Tables 59, 185 (1995).

[16] M. Warda and J. L. Egido, Phys. Rev. C 86, 014322 (2012).

[17] J. Dobaczewski, A. V. Afanasjev, M. Bender, L. M. Robledo and Yue Shi, Nucl. Phys. A 944, 388 (2015).

[18] M. Bender, K. Rutz, P.-G. Reinhard, J. A. Maruhn and W. Greiner, Phys. Rev. C 60, 034304 (1999).

[19] S. E. Agbemava, A. V. Afanasjev, T. Nakatsukasa and P. Ring, Phys. Rev. C 92, 054310 (2015).

[20] S. Goriely, A. Bauswein, and H.-T. Janka, Astrophys. J. 738, L32 (2011).

[21] O. Just, A. Bauswein, R. A. Pulpillo, S. Goriely, and H.-T. Janka, Mon. Not. R. Astron. Soc. 448, 541 (2015).

[22] L. M. Robledo and G. F. Bertsch, Phys. Rev. C 84, 054302 (2011).

[23] S. Y. Xia, H. Tao, Y. Lu, Z. P. Li, and T. Nikšić, and D. Vretenar, Phys. Rev. C 96, 054303 (2017)

[24] A.V. Afanasjev, P. Ring and I. Ragnarsson, Proc. Int. Workshop PINGST2000 "Selected topics on $N = Z$ nuclei", 2000, Lund, Sweden, Eds. D. Rudolph and M. Hellström.

[25] C. E. Svensson *et al*, Phys. Rev. Lett. 85, 2693 (2000).

[26] W. von Oertzen, M. Freer and Y. Kanada-En'yo, Phys. Rep. 432, 43 (2006).

[27] S. Åberg and L.-O. Jönsson, Z. Phys. A 349, 205 (1994).

[28] M. Freer, R. R. Betts and A. H. Wuosmaa, Nucl. Phys. A 587, 36 (1995).

[29] J.-P. Ebran, E. Khan, T. Nikšić and D. Vretenar, Phys. Rev. C 90, 054329 (2014).

[30] J. M. Yao, N. Itagaki, and J. Meng, Phys. Rev. C 90, 054307 (2014).

[31] A. V. Afanasjev and H. Abusara, Phys. Rev. C 82, 034329 (2010).

[32] Zhao, P. W. and Itagaki, N. and Meng, J., Phys. Rev. Lett. 115, 022501 (2015).

[33] J.-P. Ebran, E. Khan, T. and Nikšić and D. Vretenar, Nature 341, 487 (2012).